

## Devil's staircase formed by competing interactions stabilizing the ferroelectric smectic- $C^*$ phase and the antiferroelectric smectic- $C_A^*$ phase in liquid crystalline binary mixtures

Tadaaki Isozaki,\* Takayuki Fujikawa,† Hideo Takezoe, and Atsuo Fukuda

*Department of Organic and Polymeric Materials, Tokyo Institute of Technology, O-okayama, Meguro-ku, Tokyo 152, Japan*

Takashi Hagiwara, Yoshiichi Suzuki, and Ichiro Kawamura

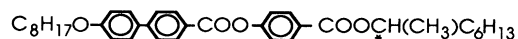
*Central Research and Development Laboratory, Showa Shell Sekiyu K.K., 123-1 Shimokawairi, Atsugi-shi, Kanagawa 243-02, Japan*

(Received 3 March 1993; revised manuscript received 25 June 1993)

In order to demonstrate experimentally that the competition between the antiferroelectric and ferroelectric interactions stabilizing  $\text{SmC}_A^*$  and  $\text{SmC}^*$  (the pairing energy of the transverse dipole moments in adjacent smectic layers and the packing entropy resulting from the excluded volume effect) produces a variety of antiferroelectric and ferrielectric subphases in the temperature region between antiferroelectric  $\text{SmC}_A^*$  and ferroelectric  $\text{SmC}^*$ , we have tried to observe the subphases in several binary mixtures of chiral smectic liquid crystals. The subphases were identified by the electric field dependence of conoscopic figures and the apparent tilt angle as a function of field strength. Systematically changing the mixing ratio of two properly chosen compounds and studying the stability of each subphase, we have substantiated that the subphases between  $\text{SmC}_A^*$  and  $\text{SmC}^*$  form a Devil's staircase,  $\text{SmC}_A^*(q_T)$ . Here,  $q_T$  is an irreducible rational number, which specifies a fraction of the ferroelectric ordering in the antiferroelectric ordering. We have also discussed the relationship of  $\text{SmC}_A^*(q_T)$  to the other staircase,  $\text{SmC}_\alpha^*(q_T)$ , that was proposed to exist as a result of the rather macroscopic, electrostatic interaction among two-dimensional spontaneous polarizations in smectic layers.

### INTRODUCTION

In 1975, Meyer *et al.*<sup>1</sup> found a novel mechanism for the formation of liquid crystalline ferroelectricity; the low symmetry of the chiral smectic- $C$  phase,  $\text{SmC}^*$ , forces the transverse dipole moments of the constituent molecules to align in a sense of the direction perpendicular to the tilting plane, leading to macroscopic polarization within a smectic layer.<sup>2</sup> Aside from slight precession from layer to layer in the tilting due to chirality, it was considered that the tilting occurs in the same direction and sense in all the layers and hence that  $\text{SmC}^*$  is ferroelectric as a whole. In 1989, however, Chandani *et al.*<sup>3</sup> noticed in 4-(1-methylheptyloxycarbonyl)phenyl 4'-octyloxybiphenyl-4-carboxylate (MHPOBC)



that there exists another antiferroelectric, smectic- $C$ -like phase, designated as  $\text{SmC}_A^*$ , where the tilting occurs in the same direction but in the opposite senses in adjacent layers, confirming that the tristable switching already observed by themselves<sup>4</sup> in 1988 is the electric-field-induced phase transition from antiferroelectric  $\text{SmC}_A^*$  to ferroelectric  $\text{SmC}^*$ . Galerne and Liebert<sup>5</sup> also reported the antiferroelectric  $\text{SmO}^*$  liquid crystal phase, confirming in the molecular scale that  $\text{SmO}^*$  has the same structure as that proposed in  $\text{SmC}_A^*$ . Quite recently, Heppke *et al.*,<sup>6</sup> Cladis and Brand,<sup>7</sup> and Takanishi *et al.*<sup>8</sup> proved that  $\text{SmO}^*$  shows the tristable switching and is miscible with  $\text{SmC}_A^*$ .

In this way, it has been well established that there exist the ferroelectric  $\text{SmC}^*$  phase and the antiferroelectric  $\text{SmC}_A^*$  phase, whose molecular unwound structures are depicted in Figs. 1(a) and 1(b), respectively. The packing entropy resulting from excluded volume effect must favor the ferroelectric  $\text{SmC}^*$  structure,<sup>9</sup> while the pairing energy of the transverse dipole moments in adjacent layers appear to stabilize the antiferroelectric  $\text{SmC}_A^*$  structure.<sup>10</sup> The purpose of this paper is to demonstrate experimentally that the competition between the packing entropy and the pairing energy produces a variety of antiferroelectric and ferrielectric subphases in the temperature region between  $\text{SmC}_A^*$  and  $\text{SmC}^*$ .

Fukui *et al.*<sup>11</sup> found two subphases which were considered closely related with  $\text{SmC}_A^*$  and  $\text{SmC}^*$ . Chandani *et al.*<sup>12</sup> designated these two subphases as  $\text{SmC}_\alpha^*$  and  $\text{SmC}_\gamma^*$  in the order of decreasing temperature. Gorecka *et al.*<sup>13</sup> soon proved that  $\text{SmC}_\gamma^*$  is a ferrielectric phase; Takezoe *et al.*<sup>14</sup> proposed its structure with the repeating

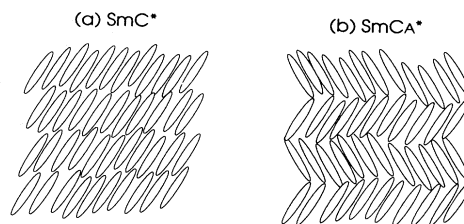
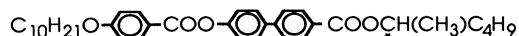


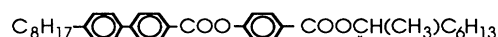
FIG. 1. Molecular unwound structures of (a) the ferroelectric  $\text{SmC}^*$  phase and (b) the antiferroelectric  $\text{SmC}_A^*$  phase.

unit of three smectic layers. Goodby and co-workers<sup>15,16</sup> also reported a similar ferrielectric phase in

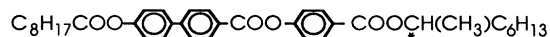


Takanishi *et al.*,<sup>10</sup> Hiraoka *et al.*,<sup>17,18</sup> and Isozaki *et al.*<sup>19</sup> insisted that  $\text{SmC}_\alpha^*$  does not represent a single structure but consists of a variety of ferrielectric and antiferroelectric structures; the Devil's staircase<sup>20,21</sup> may be formed as a result of the competition between the antiferroelectric  $P_s - P_s$  interaction and the ferroelectric one responsible for the  $\text{SmC}^*$  phase. Orihara and Ishibashi<sup>22</sup> and Sun, Orihara, and Ishibashi<sup>23</sup> have investigated the phase sequences on the basis of a Landau-type phenomenological theory. Zeks and co-workers<sup>24,25</sup> also presented the similar analysis based on a simple phenomenological model in antiferroelectric liquid crystals.

Quite recently, Okabe *et al.*<sup>26</sup> found another antiferroelectric (AF) phase in



with the phase sequence of  $\text{SmC}_A^* \leftrightarrow \text{SmC}_\gamma^* \leftrightarrow \text{AF} \leftrightarrow \text{SmC}_\alpha^* \leftrightarrow \text{SmA}$ . In a previous paper, Isozaki *et al.*<sup>27</sup> further demonstrated the appearance of ferrielectric ( $\text{FI}_L$  and  $\text{FI}_H$ ) phases in addition to the AF phase in the binary mixtures with several mixing ratios of MHPOBC and



They tried to rationalize these complicated situations by considering two staircases: One is a staircase of  $\text{SmC}_\alpha^*(q_T)$  already discussed by Takanishi *et al.*<sup>10</sup> and the other is a staircase of  $\text{SmC}_A^*(q_T)$  which is produced by the competition between the antiferroelectric and ferroelectric interactions stabilizing  $\text{SmC}_A^*$  and  $\text{SmC}^*$ , respectively. A variety of phases between  $\text{SmC}_A^*$  and  $\text{SmC}^*$ , i.e.,  $\text{SmC}_A^*$ ,  $\text{FI}_L$ ,  $\text{SmC}_\gamma^*$ ,  $\text{FI}_H$ , AF, and  $\text{SmC}^*$ , form the staircase of  $\text{SmC}_A^*(q_T)$ . Here  $q_T$  is an irreducible rational number, which specifies a fraction of the ferroelectric ordering which appears in the antiferroelectric ordering;  $\text{SmC}_\gamma^*$  and AF are designated as  $\text{SmC}_A^*(q_T = \frac{1}{3})$  and  $\text{SmC}_A^*(q_T = \frac{1}{2})$ , respectively. In the following, we will substantiate the existence of the staircase,  $\text{SmC}_A^*(q_T)$ , by carefully observing the appearance of various phases in several compounds and their binary mixtures.

## EXPERIMENT

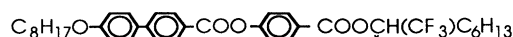
Identifying the phases as well as the transitions between them will be carried out very effectively by observing the electric field dependence of conoscopic figures<sup>13,26,27</sup> and obtaining the apparent tilt angle as a function of field strength.<sup>13,17-19,28</sup> In MHPOBC, the phase transitions thus identified have also been confirmed to occur by differential scanning calorimetry<sup>11,12</sup> (DSC) and a relaxation method,<sup>29</sup> although the thermal methods are not convenient because the enthalpy changes at the transitions are extremely small. For conoscopic observations,<sup>13,17-19,26-28</sup> we made homeotropically aligned cells using substrate glass plates treated with a surfactant

(Toray Dow Corning Silicone, AY-43-021). Two pieces of polyethylene terephthalate (PET) film covered with sheets of aluminum foil were used as spacers and electrodes. The cell thickness was 140  $\mu\text{m}$  and the electrode gap for applying an electric field was 1.8 mm. The cell was mounted in a copper oven whose temperature was controlled within an accuracy of  $\pm 0.02^\circ\text{C}$ . Conoscopic figures were observed as described previously.<sup>13</sup> An electric field was applied parallel to the smectic layer along the  $45^\circ$  direction with respect to the polarizer axes. We used an operational power supply (Hamamatsu, Regulated dc Supply Model C665) to draw the electric-field-temperature ( $E$ - $T$ ) phase diagrams.

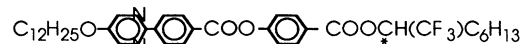
For studying the electric field dependence of apparent tilt angle in each phase, we constructed a conoscope observation system using ac voltages.<sup>28</sup> The conoscopic image projected onto a screen was taken by a CCD camera (Hitachi Electronics, KP-C210) and its output was sent to a microcomputer (NEC, PC-9801RA) through an interface board (Microtechnica, MT-9801-FMM) for the input and output of a  $512 \times 512 \times 8$  bits image. The applied ac electric field of 0.1 Hz was supplied by a wave generator (Wavetek, Model 75) through an amplifier (KEPCO, Model BOP1000M). A comparator was used to specify the voltage where an image should be recorded. The recording voltages were the maximum voltage of ac fields with variable amplitudes.

For dielectric measurements, we prepared 2  $\mu\text{m}$  thick homogeneously aligned cells. Substrate glass plates with ITO were coated with polyimide (Toray, SP-550) and rubbed unidirectionally. The dielectric measurements using an impedance analyzer (YHP 4194A) were performed by applying 0.1 Vpp, as previously described.<sup>26</sup>

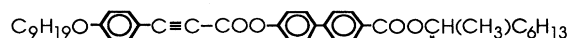
Over 3000 new chiral smectic liquid crystals have been synthesized during these 10 years, and more than 10% of them show the antiferroelectric  $\text{SmC}_A^*$  phase.<sup>30</sup> When the antiferroelectricity of some compounds is really strong, the direct phase transition between  $\text{SmA}$  and  $\text{SmC}_A^*$  occurs, as is actually observed in



and



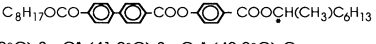
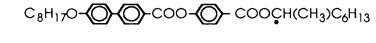
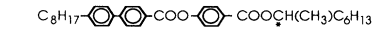
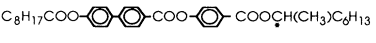
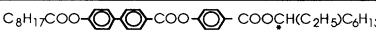
(Refs. 31 and 32, respectively). Replacing  $-\text{CH}_3$  attached to the chiral carbon by  $-\text{C}_2\text{H}_5$  further increases the antiferroelectricity in



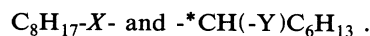
(Ref. 33). On the contrary, the very strong ferroelectricity assures the direct phase transition from  $\text{SmA}$  to  $\text{SmC}^*$ . When antiferroelectricity and ferroelectricity are well balanced and both of them are moderate in strength, successive transitions among antiferroelectric and ferrielectric phases may be observed. Table I summarizes compounds utilized in the present experiment as well as in the previous works<sup>26,27</sup> together with their phase sequences. These compounds have the same central backbone structure,



TABLE I. List of compounds and their phase transition temperatures.

<b>MHPOOCBC</b>	$C_8H_{17}OCO-$ 
	SmA-(87.2°C)-SmC <sup>*</sup> -(41.9°C)-SmC <sub>γ</sub> <sup>*</sup> -(40.0°C)-Cry.
<b>MHPOBC</b>	$C_8H_{17}O-$ 
	SmA-(120.2°C)-SmC <sub>α</sub> <sup>*</sup> -(118.7°C)-SmC <sup>*</sup> -(117.2°C)-SmC <sub>γ</sub> <sup>*</sup> -(116.3°C)-SmCA <sup>*</sup>
<b>MHPBC</b>	$C_8H_{17}-$ 
	SmA-(76.3°C)-SmC <sub>α</sub> <sup>*</sup> -(72.1°C)-AF-(66.4°C)-SmC <sub>γ</sub> <sup>*</sup> -(64.9°C)-SmCA <sup>*</sup>
<b>MHPOCBC</b>	$C_8H_{17}COO-$ 
	SmA-(105.5°C)-SmC <sub>α</sub> <sup>*</sup> -(99.5°C)-SmCA <sup>*</sup> -(73.3°C)-SmIA <sup>*</sup> -(66.1°C)-Cry.
<b>EHPOCBC</b>	$C_8H_{17}COO-$ 
	SmA-(93.3°C)-SmCA <sup>*</sup> -(66.9°C)-Cry.

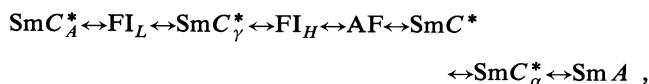
and almost the same nonchiral and chiral end chains,



Differences lie in the connection part between the non-chiral end chain and the biphenyl (-X-: -OCO-, -O-, none, -COO-) and in the residue attached to the chiral carbon (-Y-: -CH<sub>3</sub> and -C<sub>2</sub>H<sub>5</sub>). The strength of antiferroelectricity increases and hence that of ferroelectricity decreases in the listed order, as will become clear in the following.

## RESULTS

Figures 2(a)–2(h) show the  $E$ - $T$  phase diagrams in the binary mixtures of MHPOCBC with MHPOBC of various weight percent,  $R$ : (a) 0% (pure MHPOCBC), (b) 30.0%, (c) 50.0%, (d) 70.0%, (e) 80.0%, (f) 90.0%, (g) 95.0%, and (h) 100% (pure MHPOCBC). All the possible phases are



all of which appear in the case of (d)  $R = 70.0\%$ . The  $E$ - $T$  phase diagrams shown in Fig. 2 are very similar to those obtained in the binary mixture of MHPOBC and MHPOCBC.<sup>27</sup> Conoscopic figures in the ferrielectric phases,  $FI_L$ ,  $SmC_\gamma^*$ , and  $FI_H$ , are similar to one another, at least in the low-electric field region [see Fig. 3]; the centers shift toward the same direction as in  $SmC^*$  but the optic planes are parallel to the field direction under an electric field,<sup>13,26,27</sup> though the biaxiality and the apparent tilt angle in the  $FI_L$  and  $FI_H$  phases are much smaller than those in  $SmC_\gamma^*$  under the same electric field.<sup>27</sup> Conoscopic figures indicate that not only  $SmC_A^*$  but also AF are antiferroelectric, as has been already shown in Fig. 4 of Ref. 26.

Pure MHPOCBC does not have extremely strong antiferroelectricity; hence the direct transition between  $SmC_A^*$  and  $SmA$  does not occur and instead the transi-

tion via  $SmC_\alpha^*$  is observed as in Fig. 2(a). In Fig. 2(b) the  $SmC_\gamma^*$  phase emerges between  $SmC_A^*$  and  $SmC_\alpha^*$ . With increasing MHPOCBC fraction, another antiferroelectric phase (AF) appears between  $SmC_\gamma^*$  and  $SmC_\alpha^*$ , and another ferrielectric phase ( $FI_L$ ) also occurs between  $SmC_A^*$  and  $SmC_\gamma^*$ , as illustrated in Fig. 2(c). With a further increase, the  $SmC^*$  phase cuts into the boundary between AF and  $SmC_\alpha^*$  and another ferrielectric phase ( $FI_H$ ) appears between  $SmC_\gamma^*$  and AF, as shown in Fig. 2(d). Figure 2(e) resembles the phase diagram of MHPOBC,<sup>27</sup> except for the existence of AF in a narrow temperature region. Figures 2(f) and 2(g) correspond to the phase diagrams of less antiferroelectric, i.e., more ferroelectric, substances than MHPOBC. The  $SmC_\alpha^*$  phase disappears in both the phase diagrams, while the  $FI_L$  phase expands its temperature range with increasing MHPOCBC's fraction. Pure MHPOCBC has the smallest antiferroelectricity in the compounds investigated here.

By studying the apparent tilt angle in detail using the mixture of  $R = 70.0\%$  which shows the  $E$ - $T$  phase diagram given in Fig. 2(d), we noticed various ferrielectric phases in quite narrow temperature regions around  $FI_L$  and  $FI_H$ . Figures 3(a)–3(j) illustrate the electric field

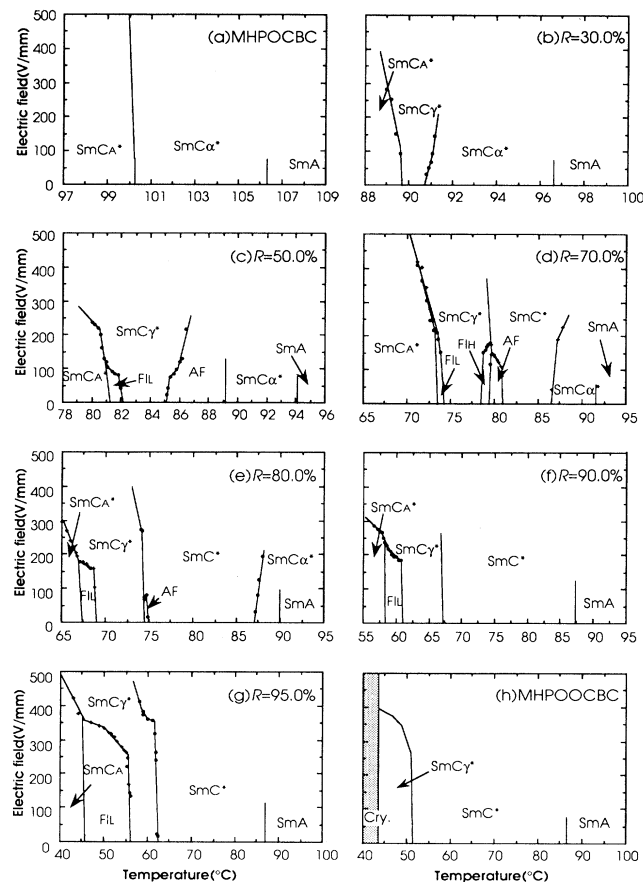


FIG. 2. The electric-field-temperature ( $E$ - $T$ ) phase diagrams of binary mixtures of MHPOCBC with MHPOBC of various weight percent,  $R$  = (a) 0% (pure MHPOCBC), (b) 30.0%, (c) 50.0%, (d) 70.0%, (e) 80.0%, (f) 90.0%, (g) 95.0%, and (h) 100% (pure MHPOCBC).

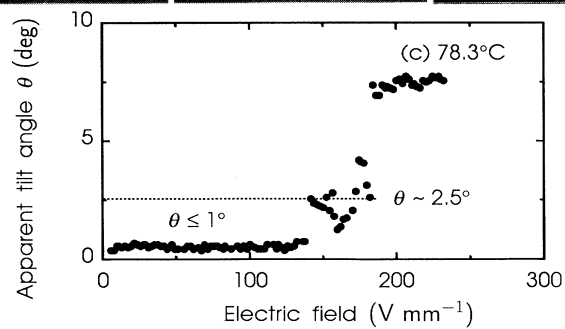
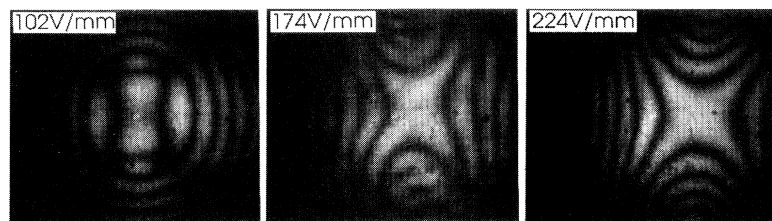
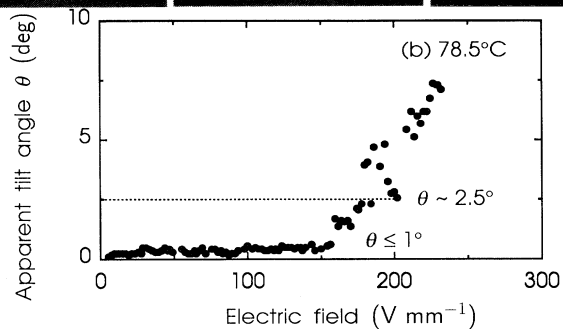
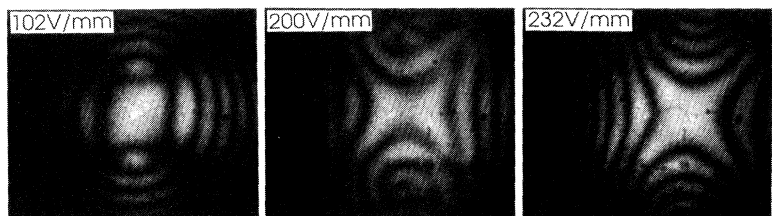
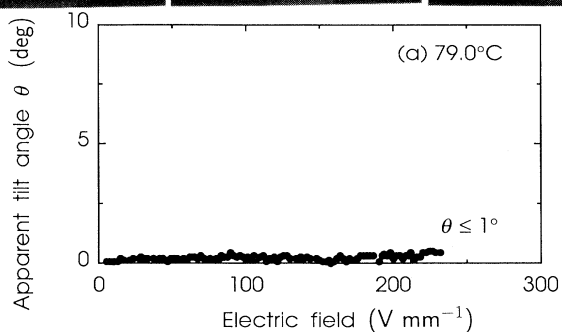
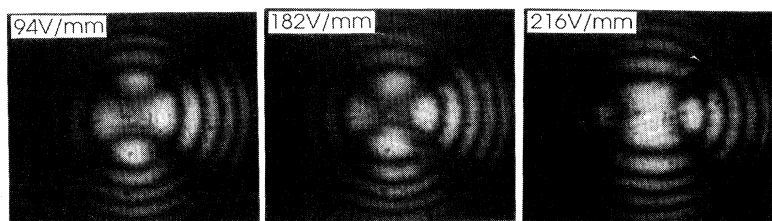


FIG. 3. The electric field dependence of apparent tilt angle in the mixture of  $R = 70.0\%$ , the  $E$ - $T$  phase diagram of which is given in Fig. 2(d), at several temperatures: (a) 79.0°C ( $FI_H$ ), (b) 78.5°C ( $FI_H$ ), (c) 78.3°C ( $FI_H$ ), (d) 78.0°C ( $FI_H$ ), (e) 77.0°C ( $SmC_\gamma^*$ ), (f) 76.0°C ( $SmC_\gamma^*$ ), (g) 75.0°C ( $SmC_\gamma^*$ ), (h) 74.2°C ( $SmC_\gamma^*$ ), (i) and (i)\* 74.0°C ( $FI_L$ ) [(i)\* was obtained by using a different cell], and (j) 73.8°C ( $SmC_A^*$ ).

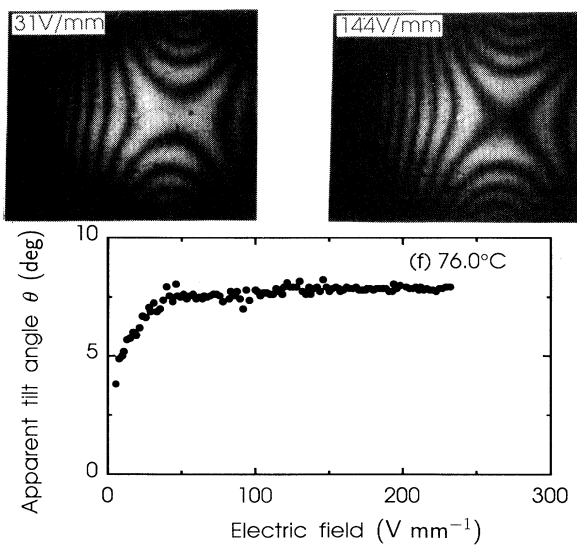
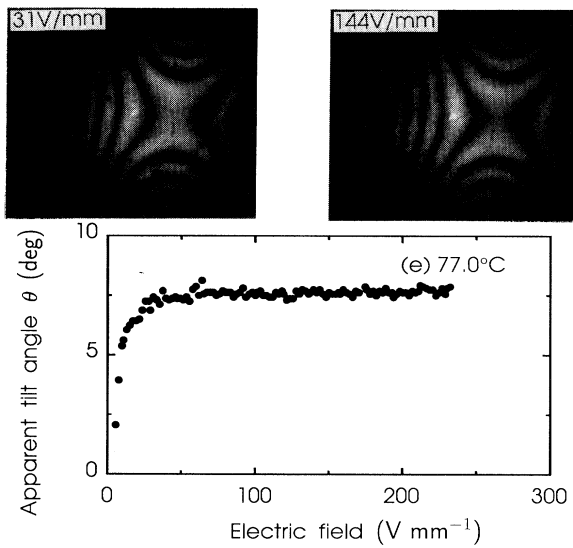
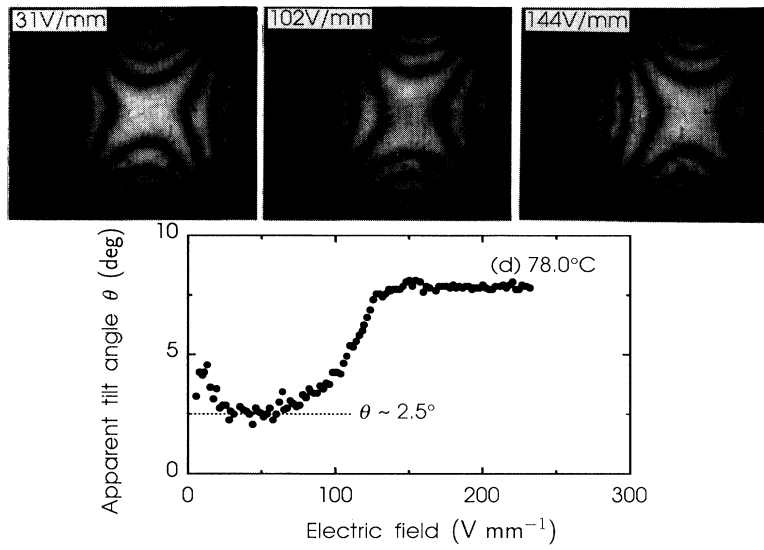


FIG. 3. (Continued).

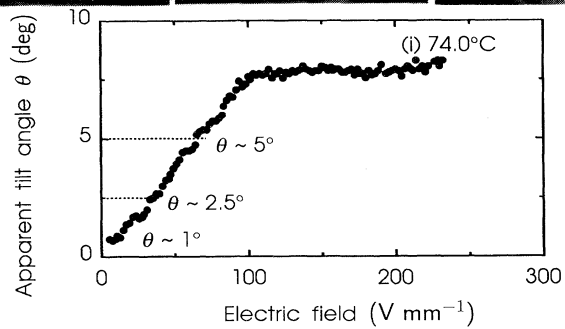
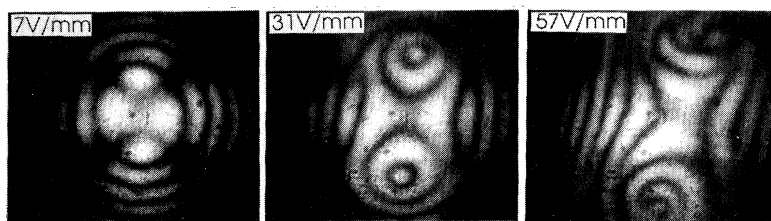
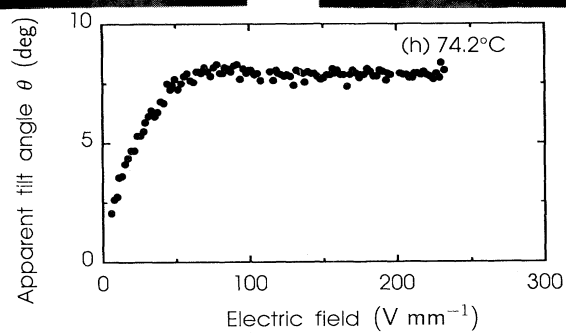
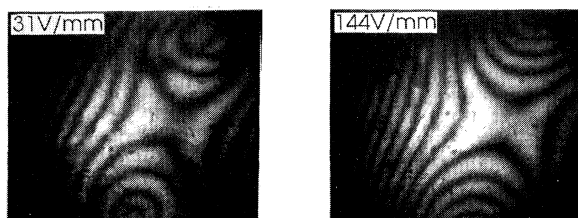
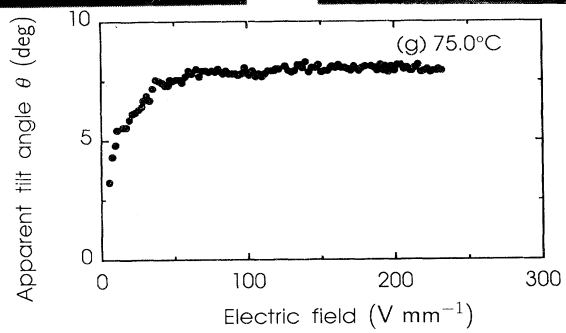
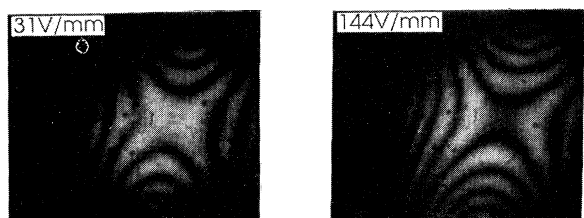


FIG. 3. (Continued).

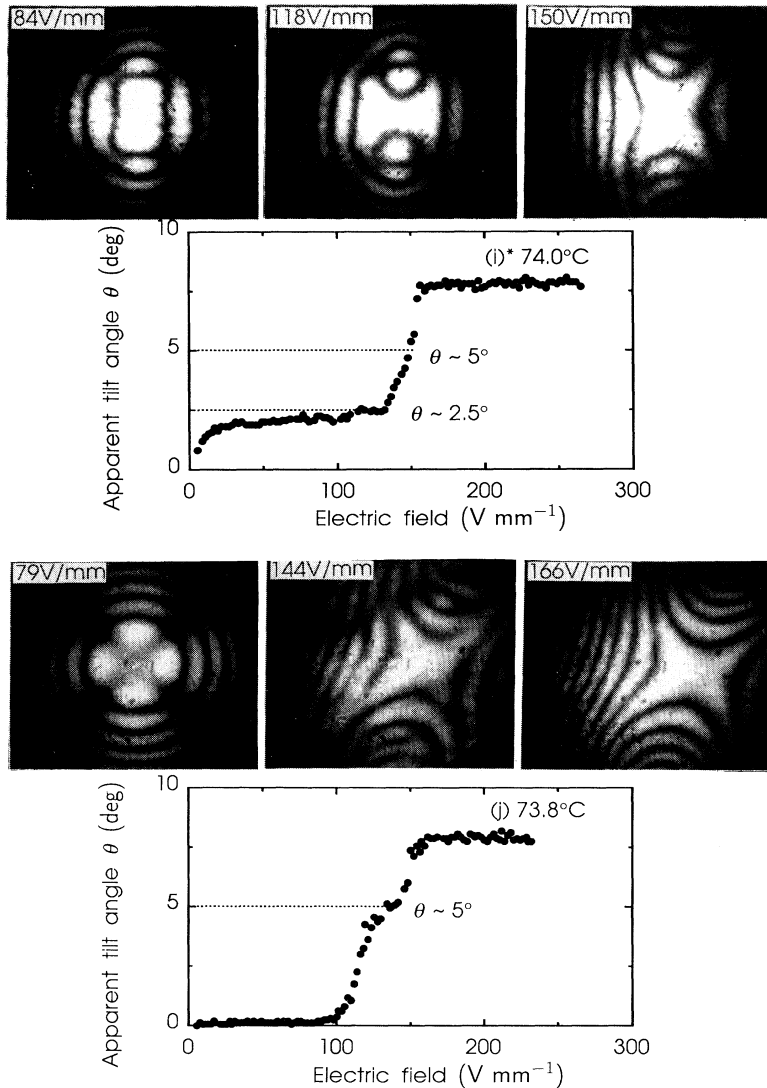


FIG. 3. (Continued).

dependence of apparent tilt angle and a series of the corresponding conoscopic figures in the vicinity of  $FI_H$  and  $FI_L$ . Figure 3(a) was obtained at 79.0°C where the phase at zero electric field was identified as  $FI_H$ . The apparent tilt angle stays very small even at 200 V/mm. The conoscopic figures are grouped into two types. In the low-field region below ca. 100 V/mm, the optic plane is parallel to the applied field as is typical of the ordinary ferroelectric phase,  $SmC_\gamma^*$ . In the high-field region above ca. 200 V/mm, on the other hand, the optic plane becomes perpendicular to the field, and the conoscopic figure is rather similar to that in the antiferroelectric  $SmC_A^*$  phase. The extremely small apparent tilt angle,  $\theta \leq 1^\circ$ , is at least partly owing to the incomplete unwinding of the helicoidal structure because of small apparent biaxiality. In  $FI_H$ , however, the optical tilt angle in the unwound helicoidal structure,  $\theta_{opt}$ , and the spontaneous polarization must be very small; hence, the molecular orientational structure in  $FI_H$  is expected to be very close to antiferroelectric, though it is actually ferroelectric.

Figures 3(b)–3(d) show the field-induced phase transi-

tion from  $FI_H$  to  $SmC_\gamma^*$ . The transition occurs not in one step but at least in two steps; the intermediate phase at an apparent tilt angle of about  $2.5^\circ$  suggests the existence of another ferroelectric phase. Three conoscopic figures illustrated correspond to these three phases; apparent biaxiality increases in the order of  $FI_H$ , intermediate phase, and  $SmC_\gamma^*$  because of partially winding structure. The intermediate phase is more clearly observed in Fig. 3(d). The conoscopic figures clearly indicate that the intermediate phase with  $\theta \sim 2.5^\circ$  shows the apparent biaxiality about equal to that in  $SmC_\gamma^*$  and hence the apparent tilt angle must be almost equal to the optical axis tilting angle,  $\theta_{opt} \approx \theta \sim 2.5^\circ$ .

Figures 3(e)–3(h) illustrate the electric field dependence of apparent tilt angle in  $SmC_\gamma^*$ . The unwinding of the helicoidal structure owing to the applying field increases rather steeply the apparent tilt angle. Not only the saturated value of the apparent tilt angle but also the minimum electric field attaining the saturation increases with descending temperature because the molecular tilt angle becomes large. The optic plane of conoscopic

figures in  $\text{SmC}_\gamma^*$  is located obliquely to the field direction and the obliqueness depends on both the field and temperature. In Figs. 3(e) and 3(f) the oblique angle is rather small and decreases with increasing field. In the low-temperature region of  $\text{SmC}_\gamma^*$ , i.e., in Figs. 3(g) and 3(h), the oblique optical plane is observed even in the high field of 144 V/mm. Although the cause for the oblique optic plane is not clear at present, these observations are not recognized to be an experimental error or a coexistence of  $\text{SmC}_\gamma^*$  and  $\text{SmC}_A^*$ .

Figure 3(i) shows electric field dependence of apparent tilt angle in  $\text{FI}_L$  and is obviously different from Figs. 3(e)–3(h) showing that in  $\text{SmC}_\gamma^*$ . Note that at least three steps are observed at about  $1^\circ$ ,  $2$ – $2.5^\circ$ , and  $5^\circ$ . To make sure this complicated electric field dependence of apparent tilt angle in  $\text{FI}_L$ , we repeated the measurements by using a different cell and obtaining Fig. 3(i)\* at the same nominal temperature. The temperature control was not accurate enough so that Fig. 3(i)\* becomes slightly different from Fig. 3(i); however, it indicates that the intermediate phase with  $\theta_{\text{opt}} \approx \theta \sim 2.5^\circ$  surely exists and that the one with  $\theta_{\text{opt}} \approx \theta \sim 5^\circ$  probably exists.

The existence of the intermediate phase with  $\theta_{\text{opt}} \sim 5^\circ$  is clearly observed in Fig. 3(j) which illustrates the electric-field-induced phase transition from  $\text{SmC}_A^*$  to  $\text{SmC}_\gamma^*$ . The conoscopic figure under 79 V/mm bears the antiferroelectric character; the optic plane is perpendicular to the field direction though the apparent biaxiality is very small.

Figure 4 summarizes the phase transition temperature at zero field as a function of weight percent  $R$  of MHPOOCBC in the mixture of MHPOOCBC and MHPOOCBC. The antiferroelectric AF phase emerges in the range of weight percent from 40% to 80%. The AF phase exists between  $\text{FI}_H$  and  $\text{SmC}^*$  on the large weight percent side, while it exists between  $\text{SmC}_\gamma^*$  and  $\text{SmC}_\alpha^*$  on the small weight percent side. These characteristic

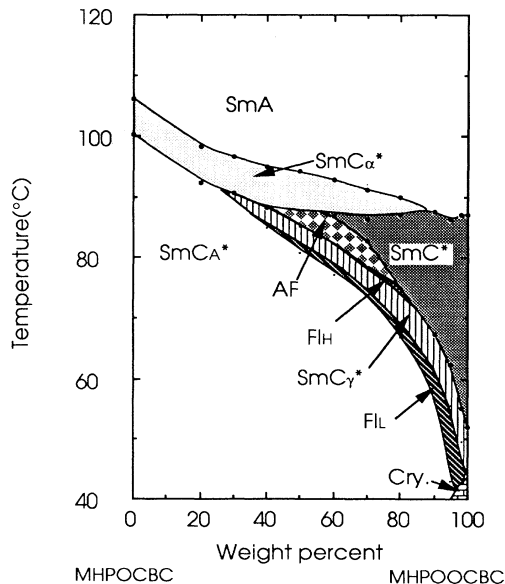


FIG. 4. The phase transition temperature at zero electric field as a function of weight percent  $R$  of MHPOOCBC in the mixture of MHPOOCBC and MHPOOCBC.

features are principally the same as those in the mixture of MHPOOCBC and MHPOOCBC.<sup>27</sup> The  $\text{FI}_L$  phase always appears between  $\text{SmC}_A^*$  and  $\text{SmC}_\gamma^*$  except for the rather small weight percent regions, and its temperature range becomes wider with increasing weight percent.

Let us next show the results of the binary mixture of MHPOOCBC and EHPOCBC. Figures 5(a)–5(h) are the  $E$ - $T$  phase diagrams of binary mixtures of EHPOCBC with MHPOOCBC of various weight percent,  $R$ : (a) 0% (pure EHPOCBC), (b) 50.0%, (c) 70.7%, (d) 80.2%, (e) 81.2%, (f) 85.0%, (g) 90.0%, and (h) 100% (pure MHPOOCBC). Only the  $\text{SmC}_A^* \leftrightarrow \text{SmA}$  phase transition is observed in Fig. 5(a), while the  $\text{SmC}_\alpha^*$  phase appears between  $\text{SmC}_A^*$  and  $\text{SmA}$  in Figs. 5(b) and 5(c). The identification of  $\text{SmC}_\alpha^*$  was made by the conoscopic figures<sup>17,19</sup> under an electric field; in the low temperature region of the  $\text{SmC}_\alpha^*$  phase a small biaxiality is observed and the optic plane is parallel to the field direction, while in the high-temperature region the biaxiality is hardly observed. Figures 5(d)–5(g) are just the same as Figs. 2(b)–2(g) and the  $E$ - $T$  phase diagrams in the previous work.<sup>27</sup> These antiferroelectric and ferroelectric phases are also observed in the regular order; in particular,

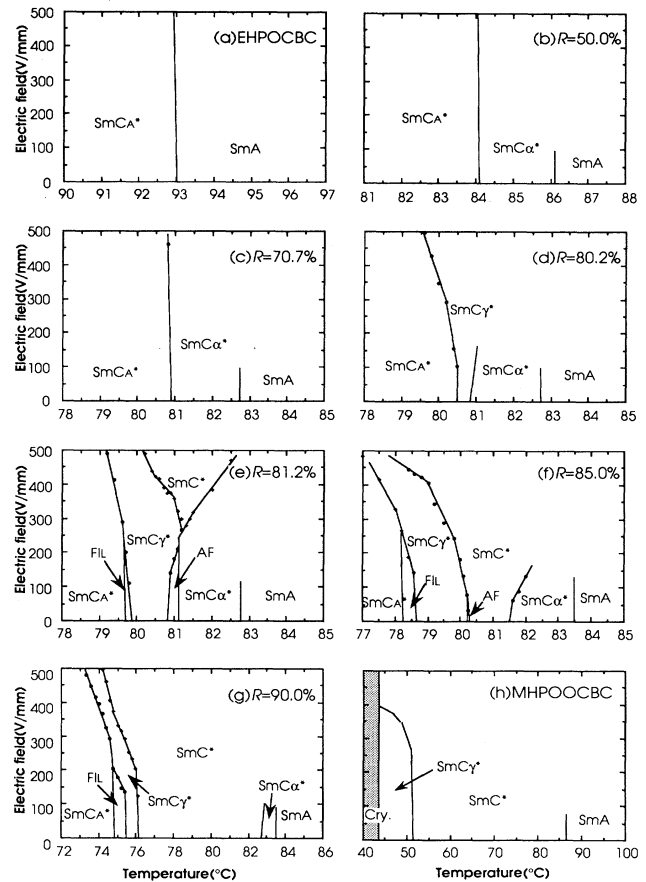


FIG. 5. The electric-field-temperature ( $E$ - $T$ ) phase diagrams of binary mixtures of EHPOCBC with MHPOOCBC of various weight percent,  $R$  = (a) 0% (pure EHPOCBC), (b) 50.0%, (c) 70.7%, (d) 80.2%, (e) 81.2%, (f) 85.0%, (g) 90.0%, and (h) 100% (pure MHPOOCBC).



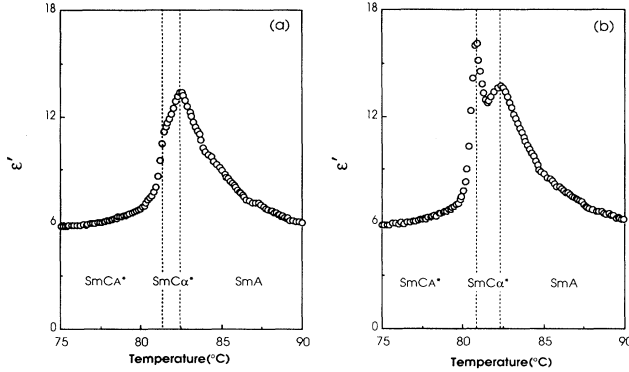


FIG. 6. The temperature dependence of dielectric constants in the mixture of  $R = 70.7\%$  at 100 Hz in the (a) heating and (b) cooling processes.

$\text{SmC}_\alpha^*$  occurs in the binary mixtures where neither of the constituent pure compounds has  $\text{SmC}_\alpha^*$ .

Figure 6 illustrates the temperature dependence of dielectric constants at 100 Hz in the mixture of  $R = 70.7\%$  in the (a) heating and (b) cooling processes. Since the transition temperatures are influenced by cell thickness, they are slightly different from the ones obtained by conoscopic observation. The  $\text{SmC}_\alpha^*$  phase is obviously noticed between  $\text{SmC}_A^*$  and  $\text{SmA}$  and the dielectric constants show a hysteresis between the heating and cooling processes in the low-temperature region of  $\text{SmC}_\alpha^*$ . The similar hysteresis has been observed in MHPOCBC.<sup>19</sup> The phase transition temperature between  $\text{SmC}_\alpha^*$  and  $\text{SmA}$  is identified by a peak in the temperature dependence. The dielectric constant becomes large toward the transition temperature at 82.5°C owing to the soft mode contribution in both the phases. The  $\text{SmC}_A^* \leftrightarrow \text{SmC}_\alpha^*$  phase transition is recognized as a steep

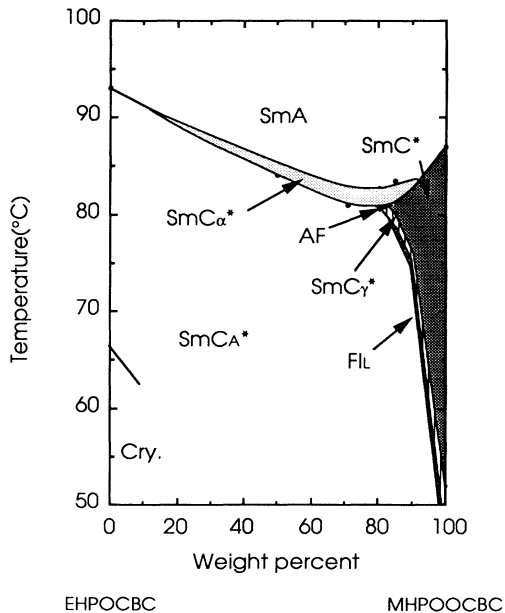


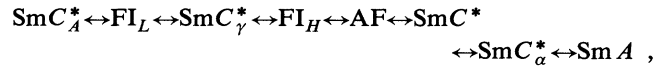
FIG. 7. The phase transition temperature at zero electric field as a function of weight percent  $R$  of MHPOCBC in the mixture of EHPOCBC and MHPOCBC.

decrease or increase in dielectric constants.

Figure 7 summarizes the phase transition temperature at zero field as a function of weight percent  $R$  of MHPOCBC in the mixture of MHPOCBC and EHPOCBC. The  $\text{SmC}_\alpha^*$  phase appears in almost all the mixing ratios  $R$ , except for the regions of the extremely small and large weight percent. The  $\text{SmC}^* \leftrightarrow \text{SmC}_\alpha^*$  phase transition is observed at rather large  $R$  (85.0 and 90.0%), and the  $\text{SmC}^*$  phase disappears when  $R$  becomes smaller than 80%. The AF phase emerges below the  $\text{SmC}_\alpha^*$  phase in a very narrow range around  $R = 80\%$ . The  $\text{SmC}_\gamma^*$  phase exists in the region where  $R$  is larger than 80% and its temperature range is narrow. The temperature range of  $\text{SmC}_\alpha^*$  in Fig. 7 is narrower than that in Fig. 4. In this way, the appearance of the subphases in Fig. 7 occurs not only in the reduced temperature ranges but also in the much more restricted weight percent regions, as compared with that in Fig. 4.

## DISCUSSION

The three binary systems so far studied give the similar  $E$ - $T$  phase diagrams. All the possible phases observed stably at zero electric field are



and this order has never changed. Near the ferroelectric phases  $\text{FI}_L$  and  $\text{FI}_H$  there appear to exist a few additional ferroelectric phases. When a substance has very strong antiferroelectricity, it exhibits the direct phase transition,  $\text{SmC}_A^* \leftrightarrow \text{SmA}$ . As the antiferroelectricity decreases, the  $\text{SmC}^* \leftrightarrow \text{SmA}$  transition is to occur; because of the  $P_s$ - $P_s$  interaction, however,  $\text{SmC}_\alpha^*$  squeezes itself between  $\text{SmC}_A^*$  and  $\text{SmA}$ . With a further decrease in antiferroelectricity or a further increase in ferroelectricity, first the transition  $\text{SmC}_\gamma^* \leftrightarrow \text{SmC}_\alpha^*$ , then the transition  $\text{AF} \leftrightarrow \text{SmC}_\alpha^*$ , and finally the transition  $\text{SmC}^* \leftrightarrow \text{SmC}_\alpha^*$  become to occur after some development within  $\text{SmC}_\alpha^*$  which may result in the Devil's staircase,  $\text{SmC}_\alpha^*(q_T)$ .<sup>10,17-21</sup> When antiferroelectricity and ferroelectricity are well balanced and both of them are moderate in strength, all the possible phases appear in the order described above. As the ferroelectricity becomes much stronger, first AF, then  $\text{SmC}_\alpha^*$ , and finally  $\text{SmC}_\gamma^*$  disappears, and the direct transition  $\text{SmC}_A^* \leftrightarrow \text{SmC}^*$  occurs. In a mixture which consists of two compounds with really strong antiferroelectricity and ferroelectricity, no subphases may be observed and the  $\text{SmC}_A^* \leftrightarrow \text{SmC}^*$  direct transition may occur even when both of the electricity are well balanced.

As has already been described in  $\text{SmC}_\alpha^*(q_T)$  by Takahashi *et al.*,<sup>10</sup> the competition between antiferroelectricity and ferroelectricity resulting in the appearance of the subphases  $\text{FI}_L$ ,  $\text{SmC}_\gamma^*$ ,  $\text{FI}_H$ , and AF, may be characterized phenomenologically by the one-dimensional Ising model with long-range repulsive interactions<sup>21</sup> whose energy is given by

$$E = - \sum_i HS_i + \sum_{i,j} J(i-j)(S_i + \frac{1}{2})(S_j + \frac{1}{2}).$$

The spin-down state,  $S_i = -\frac{1}{2}$ , represents the antiferroelectric ordering (designated as  $A$ ) of the neighboring smectic layers and the spin-up state,  $S_i = +\frac{1}{2}$ , the ferroelectric ordering (designated as  $F$ ). The interaction  $J(i-j)$  is the repulsive one between the  $F$  orderings, and the background,  $H = H_A - H_F$ , is a measure of the stability of  $F$  defects; the  $H_F$  term represents the packing entropy resulting from the excluded volume effect that depends on temperature,<sup>9</sup> and the  $H_A$  term is the pairing energy of the transverse dipole moments in adjacent layers.<sup>10</sup> Any subphase structure expected to appear is specified by an irreducible rational number  $q_T$ , which constitutes a Farey sequence given in Fig. 8. Some of the structures specified by simple rational numbers are illustrated in the upper part of the figure. The structure with  $q_T = m/n$  is antiferroelectric when either  $m$  or  $n$  is even; otherwise it represents a ferroelectric phase with spontaneous polarization,  $P_s(\text{ferro})/n$ , where  $P_s(\text{ferro})$  is the

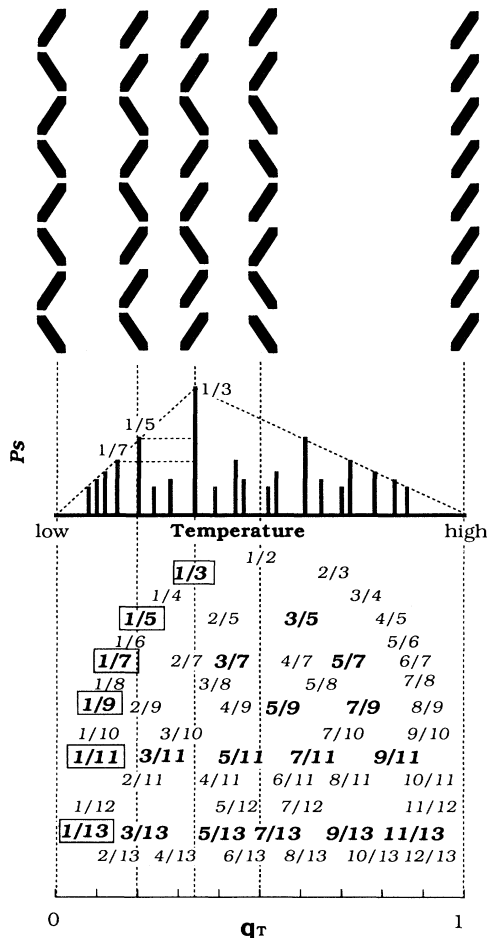


FIG. 8. The irreducible fraction numbers,  $q_T$ 's, constitute the Farey sequence. The numbers representing the ferroelectric structures are shown as bold and italic letters and those representing the antiferroelectric structures are shown as ordinary italic letters. The corresponding spontaneous polarizations,  $P_s$ 's, are indicated by bars at  $q_T$ 's on the abscissa of unit length. Some of the structures specified by simple rational numbers are illustrated in the upper part of the figure.

expected spontaneous polarization of the corresponding ferroelectric structure ( $q_T = 1$ ) with the same molecular tilt angle. Note that  $\theta(\text{ferro})/n$  approximately represents the tilting angle of the optical axis,  $\theta_{\text{opt}}(q_T = m/n)$ , i.e., the apparent tilt angle when the helicoidal structure is unwound completely. One of the characteristic features of this staircase is that the packing entropy plays an important role in its formation.

It is quite reasonable to assign the two rather stable subphases,  $\text{SmC}_\gamma^*$  and AF, to  $\text{SmC}_A^*(q_T = \frac{1}{3})$  and  $\text{SmC}_A^*(q_T = \frac{1}{2})$ . Naturally,  $\text{SmC}_A^*(q_T = \frac{1}{2})$  is antiferroelectric. In ferroelectric  $\text{SmC}_A^*(q_T = \frac{1}{3})$ , the antiferroelectric and ferroelectric orderings have nearly the same energy. The helicoidal pitch is expected to be long because the helicoidal pitch of  $\text{SmC}_A^*(q_T = 0)$  consisting of the  $A$  ordering only and that of  $\text{SmC}_A^*(q_T = 1)$ , i.e.,  $\text{SmC}^*$ , consisting of the  $F$  ordering only are nearly equal to each other but their handedness is just opposite. Hence solitonlike defects produced by misplacing the  $A$  and  $F$  orderings must be thermally excited here and there to neutralize the spontaneous polarization spatially, causing fluctuations in  $\text{SmC}_A^*(q_T = \frac{1}{3})$ . The fluctuations may explain the low-frequency dielectric responses in  $\text{SmC}_\gamma^*$  observed by Glogarova *et al.*<sup>34</sup> and the very slow relaxation time observed by Miyachi<sup>35</sup> in dynamic Rayleigh light scattering.

The intermediate phase with  $\theta_{\text{opt}} \sim 5^\circ$  near  $\text{FI}_L$  observed in Figs. 3(i), 3(i)\*, and 3(j) may probably correspond to  $\text{SmC}_A^*(q_T = \frac{1}{5})$ ; the phase with  $\theta_{\text{opt}} \sim 2.5^\circ$  near  $\text{FI}_H$  observed stably in Fig. 3(d) and intermediately during transition to  $\text{SmC}_\gamma^*$ , i.e.,  $\text{SmC}_A^*(q_T = \frac{1}{3})$ , in Figs. 3(b) and 3(c) must be  $\text{SmC}_A^*(q_T = \frac{2}{7})$ , which is the simplest ferroelectric structure between  $q_T = \frac{1}{3}$  and  $\frac{1}{2}$ . Then it is possible to assign the small step in Fig. 3(i) and the stable phase with  $\theta_{\text{opt}} \sim 2.5^\circ$  in Fig. 3(i)\* to  $\text{SmC}_A^*(q_T = \frac{1}{7})$ . The simplest  $q_T$  for the stable phases observed in Figs. 3(a)–3(c) is  $\frac{5}{11}$ . A rather simple possible  $q_T$  for the intermediate phase with  $\theta \sim 1^\circ$  in Fig. 3(i) is  $\frac{1}{9}$ ,  $\frac{1}{11}$ , or  $\frac{3}{11}$ . An alternation of the optic plane from parallel to perpendicular to the applied field observed in Fig. 3(a) may result from very small spontaneous polarization in the ferroelectric phase.

The interaction through the spontaneous polarization is linearly proportional to an electric field, while the interaction through the dielectric anisotropy shows quadratic dependence on an electric field. Moreover, the tilt planes of the unwound structures by these interactions are perpendicular to each other. It may also be responsible for the optic planes oblique to the field direction observed in  $\text{FI}_L$  and on the low-temperature side of  $\text{SmC}_\gamma^*$ . Anyway, the present experiment is not accurate enough to study the subphases other than  $\text{SmC}_\gamma^*$  and AF. We have to prevent the sample degradation resulting in the change of phase transition temperatures and at the same time to improve the temperature control accuracy. Sample purity may become another obstacle; we may have to perform the similar experiment by using not mixtures but suitable pure compounds; optimistically, however, we may still be allowed to use mixtures, because the transi-

tions between the subphases are expected to occur in exceptionally narrow temperature widths of the order of 1 mK even in mixtures as Ema *et al.*<sup>29</sup> quite recently showed in a pure compound, MHPOBC.

In this way, it becomes clear that there exist two staircases; one is  $\text{Sm}C_A^*(q_T)$  and the other is  $\text{Sm}C_\alpha^*(q_T)$ . When  $\text{Sm}C^*$  exists stably at zero electric field, the competition between antiferroelectricity and ferroelectricity is apparently obvious not only in  $\text{Sm}C_A^*(q_T)$  as described above but also in  $\text{Sm}C_\alpha^*$  because at least the high-temperature region of  $\text{Sm}C_\alpha^*$  is antiferroelectric and its low-temperature side is bounded by  $\text{Sm}C^*$ . A question arises: Why the ferroelectricity increases with rising temperature in  $\text{Sm}C_A^*(q_T)$  while it does with falling temperature in  $\text{Sm}C_\alpha^*(q_T)$ . An answer to this question is the tilt angle change. Since the phase transition from  $\text{Sm}A$  is of the second order or of the weakly first order, the tilt angle increases from almost zero in  $\text{Sm}C_\alpha^*(q_T)$ . An increase in the tilt angle must enhance the excluded volume effect which promotes the formation of the ferroelectric ordering.

In subphases specified by  $q_T > \frac{1}{2}$ , the  $A$  orderings appear as the likes of defects in the  $F$  orderings. Figure 9 illustrates some examples. A reasonably strong electric field can remove some of these defectlike  $A$  orderings rather easily, resulting in a state with a large spontaneous polarization and a large optical axis tilt angle. The  $E$ - $T$  phase diagrams so far obtained unambiguously indicate that subphases specified by  $q_T > \frac{1}{2}$  could not be observed in  $\text{Sm}C_A^*(q_T)$  when  $\text{Sm}C^*$  is stable. When other phases with  $q_T = 0, \frac{1}{3},$  and  $\frac{1}{2}$ , i.e.,  $\text{Sm}C_A^*, \text{Sm}C_\gamma^*$ , and AF are bordered with  $\text{Sm}C_\alpha^*$ , it is not easy to decide conclusively whether the region identified as the low-temperature part of  $\text{Sm}C_\alpha^*$  is actually  $\text{Sm}C_\alpha^*(q_T)$  or  $\text{Sm}C_A^*(q_T)$  with  $q_T > \frac{1}{2}$ . In a previous paper, Isozaki *et al.*<sup>19</sup> analyzed the conoscopic figures in (*R*)-MHPOCBC on the basis of  $\text{Sm}C_\alpha^*(q_T)$ . Takanishi<sup>36</sup> observed the switching current and light transmission by applying a square-wave electric field in the same compound and confirmed the existence of several ferroelectric and antiferroelectric phases at zero field, supporting the occurrence of  $\text{Sm}C_\alpha^*(q_T)$ . Anyway, because of its structural complexity, it must take a long time for a subphase with  $q_T > \frac{1}{2}$  to be formed after changing the temperature; hence, the hysteresis is observed in the dielectric responses. In other words, the hysteresis suggests the structural complexity and hence the formation of the staircase,  $\text{Sm}C_\alpha^*(q_T)$ .

It is not factitious to consider the  $P_s$ - $P_s$  interaction, because any tilting of the molecular long axis in the same direction and sense produces the spontaneous polarization in a smectic layer. Once the layer spontaneous polarization is produced, there must exist rather macroscopic electrostatic interaction among the smectic layers. At least when  $\text{Sm}C_A^*$  occurs stably, the smectic-layer structure must be much closer to the ordinary picture of molecules lying on equidistant planes<sup>36</sup> rather than to the sinusoidal density wave depicted in Fig. 3 of Ref. 37 by Schätzing and Litster; otherwise, it could not be decided in which of the two possible senses may tilt the molecules in the minimum density region. Therefore, the electro-

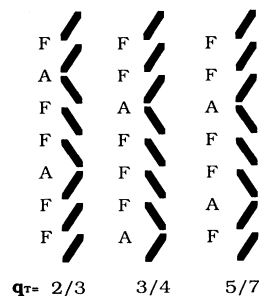


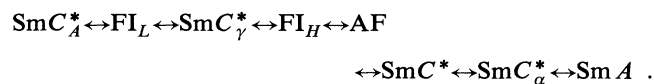
FIG. 9. Some of the structures with  $q_T > \frac{1}{2}$ .

static  $P_s$ - $P_s$  interaction promotes the formation of the antiferroelectric structure,  $\text{Sm}C_\alpha^*(q_T=0)$ , on the high temperature side of  $\text{Sm}C_\alpha^*$  where the molecular tilt angle and hence the excluded volume effect are small. Recently, Beresnev *et al.*<sup>38</sup> and Haase *et al.*<sup>39</sup> discussed several novel modulated structures caused by the electrostatic  $P_s$ - $P_s$  interaction, performing detailed electrooptical measurements and dielectric investigations. A probable reason why they did not observe the antiferroelectric structure, i.e.,  $\text{Sm}C_\alpha^*(q_T=0)$ , is that the substances they used have smectic layer structures closer to the sinusoidal density wave than our substances exhibiting  $\text{Sm}C_\alpha^*$ .

## CONCLUSIONS

Observing the conoscopic figures under an applied electric field and drawing the electric-field-temperature ( $E$ - $T$ ) phase diagrams, we have found a variety of  $\text{Sm}C^*$ -like subphases in the temperature region between antiferroelectric  $\text{Sm}C_A^*$  and ferroelectric  $\text{Sm}C^*$  in several binary mixtures. The binary systems so far studied give a series of the  $E$ - $T$  phase diagrams.

(1) All the possible phases observed stably at zero electric field are



Some of the phases may not actually occur but, when they do exist, they exactly follow this order. Near the ferroelectric phase  $\text{FI}_L$  and  $\text{FI}_H$ , there appear to exist a few additional ferroelectric phases.

(2) Any antiferroelectric liquid-crystalline substance, whether it is a pure compound or a mixture, may exhibit a similar pattern of the  $E$ - $T$  phase diagram which can be found in the series illustrated in Figs. 2 and 5.

(3) The pattern of the  $E$ - $T$  phase diagram mainly depends on the relative strength of the antiferroelectric and ferroelectric interactions stabilizing  $\text{Sm}C_A^*$  and  $\text{Sm}C^*$ , respectively, at least when both of the interactions are moderate in strength.

(4) The relative strength is a monotonic function of the mixing ratio of binary mixtures, and hence the phase diagrams showing transition temperatures vs mixing ratio illustrated in Figs. 4 and 7 clearly indicate how the succes-

sive phase transitions vary with the relative strength.

(5) If a substance has strong antiferroelectricity or ferroelectricity, it exhibits the direct phase transition,  $\text{SmC}_A^* \leftrightarrow \text{Sm}A$  or  $\text{SmC}^* \leftrightarrow \text{Sm}A$ . When antiferroelectricity and ferroelectricity are well balanced and moderate in strength, all the possible phases appear in the order described above.

(6) We have concluded that the subphases other than  $\text{SmC}_\alpha^*$  results from the competition between the antiferroelectric and ferroelectric interactions stabilizing  $\text{SmC}_A^*$  (the pairing energy of transverse dipole moments in adjacent smectic layers) and  $\text{SmC}^*$  (the packing entropy resulting from the excluded volume effect), forming a

Devil's staircase,  $\text{SmC}_A^*(q_T)$ .

(7) We have also discussed the relationship of  $\text{SmC}_A^*(q_T)$  to the other staircase,  $\text{SmC}_\alpha^*(q_T)$ , that was proposed to exist as a result of the rather macroscopic, electrostatic interaction among two-dimensional spontaneous polarizations in smectic layers.

#### ACKNOWLEDGMENTS

This work was partially supported by the Grant-in-Aid for Scientific Research (No. 05402026) from the Ministry of Education, Science and Culture and the Casio Science Promotion Foundation.

- \*On leave of absence from Central Research and Development Laboratory, Showa Shell Sekiyu K.K., 123-1 Shimokawairi, Atsugi-shi, Kanagawa 243-02, Japan.
- †Present address: Display Device Research Section, Nippon-denso Co. Ltd., 1 Shimohazumi-cho, Nishio-shi, Aichi 445, Japan.
- <sup>1</sup>R. B. Meyer, L. Liebert, L. Strzelecki, and P. Keller, *J. Phys. (Paris)* **36**, L69 (1975).
- <sup>2</sup>R. B. Meyer, *Mol. Cryst. Liq. Cryst.* **40**, 33 (1977).
- <sup>3</sup>A. D. L. Chandani, E. Gorecka, Y. Ouchi, H. Takezoe, and A. Fukuda, *Jpn. J. Appl. Phys.* **28**, L1265 (1989).
- <sup>4</sup>A. D. L. Chandani, T. Hagiwara, Y. Suzuki, Y. Ouchi, H. Takezoe, and A. Fukuda, *Jpn. J. Appl. Phys.* **27**, L729 (1988).
- <sup>5</sup>Y. Galerne and L. Liebert, *Phys. Rev. Lett.* **66**, 2891 (1991).
- <sup>6</sup>G. Heppke, P. Kleinberg, D. Löttsch, S. Mery, and R. Schashidhar, *Mol. Cryst. Liq. Cryst. Lett.* (to be published).
- <sup>7</sup>P. E. Cladis and H. R. Brand, *Liq. Cryst.* **14**, 1327 (1993).
- <sup>8</sup>Y. Takanishi, H. Takezoe, M. Johno, T. Yui, and A. Fukuda, *Jpn. J. Appl. Phys.* (to be published).
- <sup>9</sup>M. Nakagawa, *J. Phys. Soc. Jpn.* (to be published).
- <sup>10</sup>Y. Takanishi, K. Hiraoka, V. K. Agrawal, H. Takezoe, A. Fukuda, and M. Matsushita, *Jpn. J. Appl. Phys.* **30**, 2023 (1991).
- <sup>11</sup>M. Fukui, H. Orihara, Y. Yamada, N. Yamamoto, and Y. Ishibashi, *Jpn. J. Appl. Phys.* **28**, L849 (1989).
- <sup>12</sup>A. D. L. Chandani, Y. Ouchi, H. Takezoe, A. Fukuda, K. Terashima, K. Furukawa, and A. Kishi, *Jpn. J. Appl. Phys.* **28**, L1261 (1989).
- <sup>13</sup>E. Gorecka, A. D. L. Chandani, Y. Ouchi, H. Takezoe, and A. Fukuda, *Jpn. J. Appl. Phys.* **29**, 131 (1990).
- <sup>14</sup>H. Takezoe, J. Lee, Y. Ouchi, and A. Fukuda, *Mol. Cryst. Liq. Cryst.* **202**, 85 (1991).
- <sup>15</sup>J. W. Goodby, *J. Mater. Chem.* **1**, 307 (1992).
- <sup>16</sup>J. W. Goodby, J. S. Patel, and E. Chin, *J. Mater. Chem.* **2**, 197 (1992).
- <sup>17</sup>K. Hiraoka, Y. Takanishi, K. Skarp, H. Takezoe, and A. Fukuda, *Jpn. J. Appl. Phys.* **30**, L1819 (1991).
- <sup>18</sup>K. Hiraoka, Y. Takanishi, H. Takezoe, A. Fukuda, T. Isozaki, Y. Suzuki, and I. Kawamura, *Jpn. J. Appl. Phys.* **31**, 3394 (1992).
- <sup>19</sup>T. Isozaki, K. Hiraoka, Y. Takanishi, H. Takezoe, A. Fukuda, Y. Suzuki, and I. Kawamura, *Liq. Cryst.* **12**, 59 (1992).
- <sup>20</sup>P. Bak, *Rep. Prog. Phys.* **45**, 587 (1982).
- <sup>21</sup>P. Bak, *Phys. Today* **39**, No. 12, 38 (1986).
- <sup>22</sup>H. Orihara and Y. Ishibashi, *Jpn. J. Appl. Phys.* **29**, L115 (1990).
- <sup>23</sup>H. Sun, H. Orihara, and Y. Ishibashi, *J. Phys. Soc. Jpn.* **60**, 4175 (1991).
- <sup>24</sup>B. Zeks, R. Blinc, and M. Cepic, *Ferroelectrics* **122**, 221 (1991).
- <sup>25</sup>B. Zeks and M. Cepic, *Liq. Cryst.* **14**, 445 (1993).
- <sup>26</sup>N. Okabe, Y. Suzuki, I. Kawamura, T. Isozaki, H. Takezoe, and A. Fukuda, *Jpn. J. Appl. Phys.* **31**, L793 (1992).
- <sup>27</sup>T. Isozaki, T. Fujikawa, H. Takezoe, A. Fukuda, T. Hagiwara, Y. Suzuki, and I. Kawamura, *Jpn. J. Appl. Phys.* **31**, L1435 (1992).
- <sup>28</sup>T. Fujikawa, K. Hiraoka, T. Isozaki, K. Kajikawa, H. Takezoe, and A. Fukuda, *Jpn. J. Appl. Phys.* **32**, 985 (1993).
- <sup>29</sup>K. Ema, H. Yao, I. Kawamura, T. Chan, and C. W. Garland, *Phys. Rev. E.* **47**, 1203 (1993).
- <sup>30</sup>*Future Liquid Crystal Display and its Materials*, edited by A. Fukuda (CMC, Tokyo, 1992) [in Japanese]. This reference contains a rather comprehensive list of antiferroelectric liquid crystals synthesized before 1991.
- <sup>31</sup>Y. Suzuki, T. Hagiwara, I. Kawamura, N. Okamura, T. Kitazume, M. Kakimoto, Y. Imai, Y. Ouchi, H. Takezoe, and A. Fukuda, *Liq. Cryst.* **5**, 167 (1989).
- <sup>32</sup>S. Inui, S. Kawano, M. Saito, H. Iwane, Y. Takanishi, K. Hiraoka, Y. Ouchi, H. Takezoe, and A. Fukuda, *Jpn. J. Appl. Phys.* **29**, L987 (1990).
- <sup>33</sup>I. Nishiyama, Ph.D. thesis, the University of Hull, 1992.
- <sup>34</sup>M. Glogarova, H. Sverenyak, A. Fukuda, and H. Takezoe, *Liq. Cryst.* **14**, 463 (1993).
- <sup>35</sup>K. Miyachi, Master thesis (in Japanese), Tokyo Institute of Technology, 1993.
- <sup>36</sup>Y. Takanishi, Ph.D. thesis (in Japanese), Tokyo Institute of Technology, 1993.
- <sup>37</sup>R. Schätzing and J. D. Litster, in *Advances in Liquid Crystals*, edited by G. H. Brown (Academic, New York, 1979), p. 145.
- <sup>38</sup>L. A. Beresnev, M. V. Loseva, N. I. Chernova, S. G. Kononov, P. V. Adomenas, and E. P. Pozhidayev, *Pis'ma Zh. Eksp. Teor. Fiz.* **51**, 457 (1990).
- <sup>39</sup>W. Haase, S. Hiller, M. Pfeiffer, and L. A. Beresner, *Ferroelectrics* (to be published).

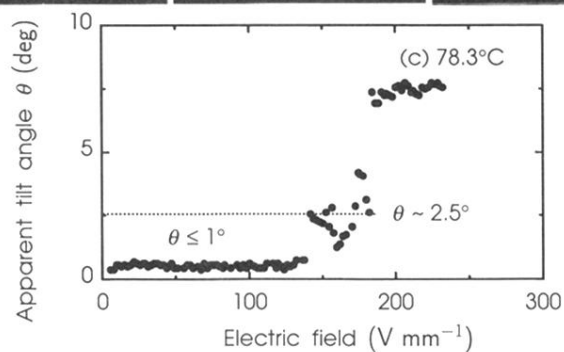
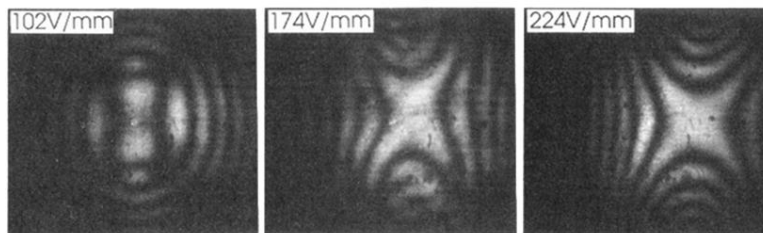
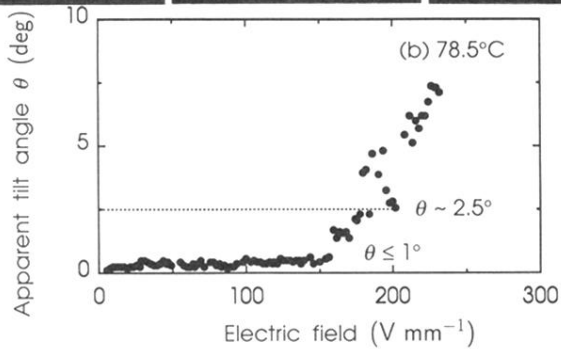
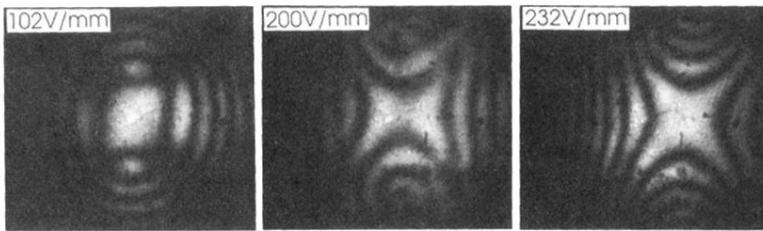
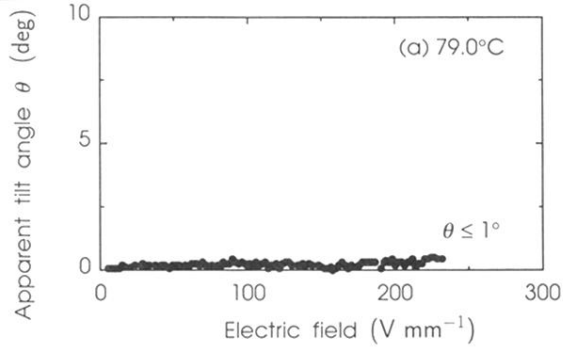
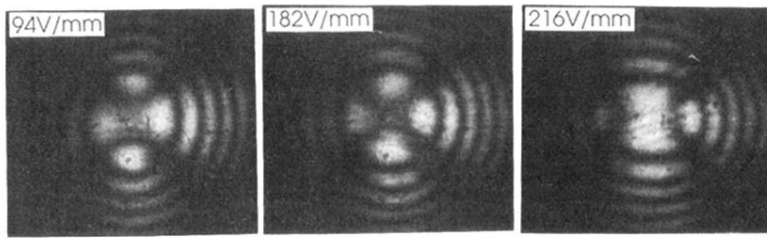


FIG. 3. The electric field dependence of apparent tilt angle in the mixture of  $R = 70.0\%$ , the  $E$ - $T$  phase diagram of which is given in Fig. 2(d), at several temperatures: (a)  $79.0^\circ\text{C}$  ( $\text{FI}_H$ ), (b)  $78.5^\circ\text{C}$  ( $\text{FI}_H$ ), (c)  $78.3^\circ\text{C}$  ( $\text{FI}_H$ ), (d)  $78.0^\circ\text{C}$  ( $\text{FI}_H$ ), (e)  $77.0^\circ\text{C}$  ( $\text{SmC}_\gamma^*$ ), (f)  $76.0^\circ\text{C}$  ( $\text{SmC}_\gamma^*$ ), (g)  $75.0^\circ\text{C}$  ( $\text{SmC}_\gamma^*$ ), (h)  $74.2^\circ\text{C}$  ( $\text{SmC}_\gamma^*$ ), (i) and (i)\*  $74.0^\circ\text{C}$  ( $\text{FI}_L$ ) [(i)\* was obtained by using a different cell], and (j)  $73.8^\circ\text{C}$  ( $\text{SmC}_A^*$ ).

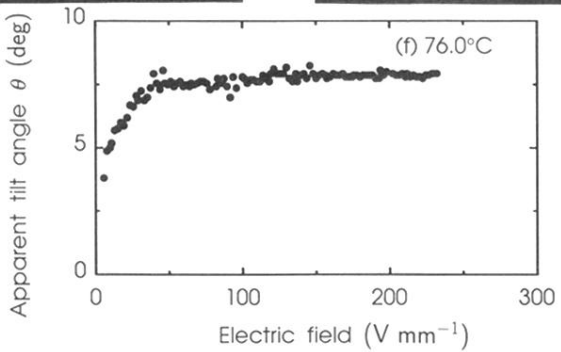
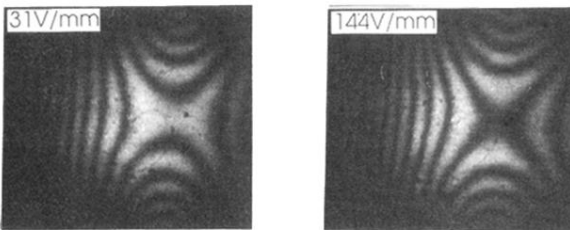
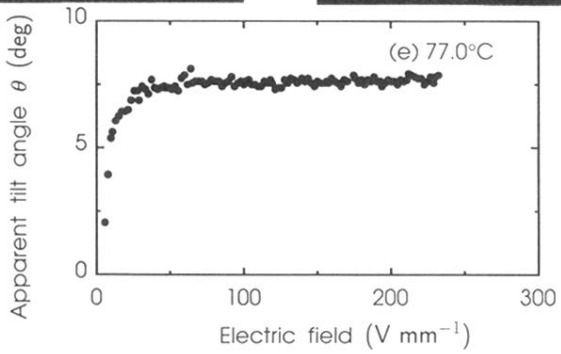
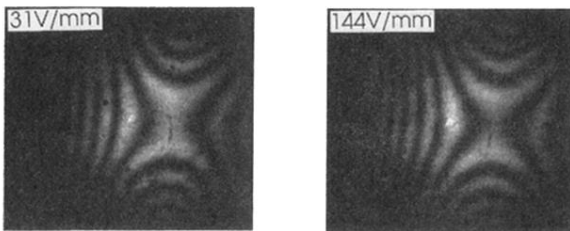
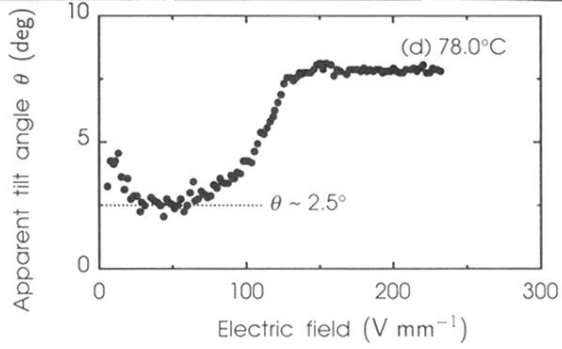
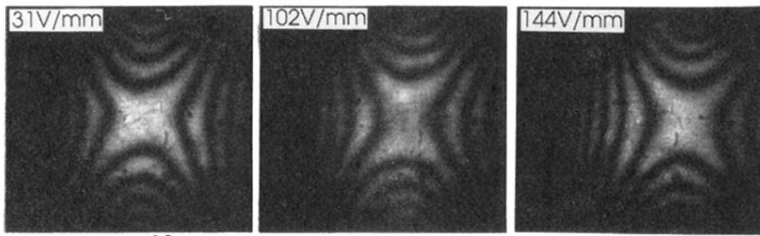


FIG. 3. (Continued).

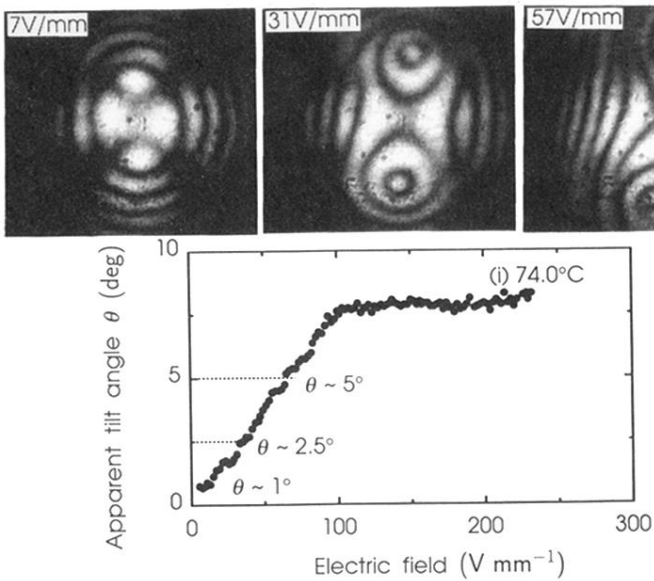
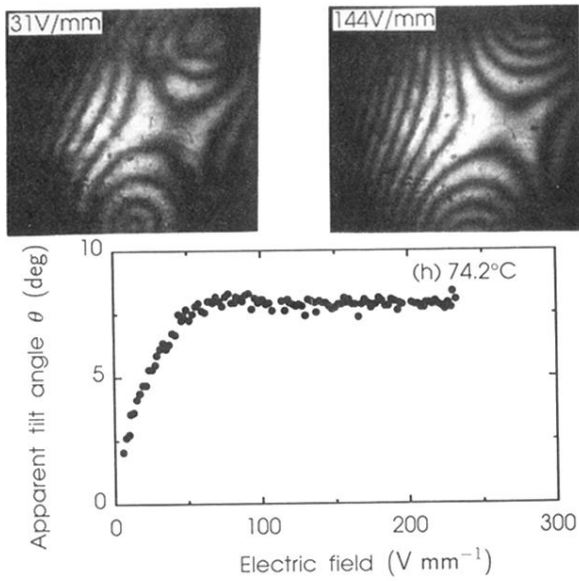
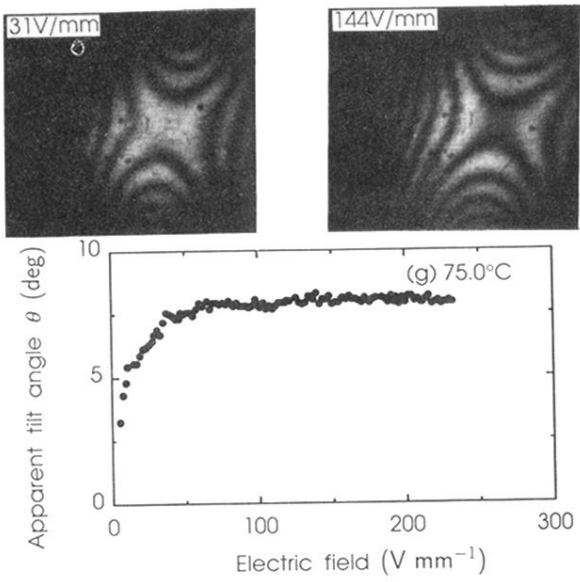


FIG. 3. (Continued).

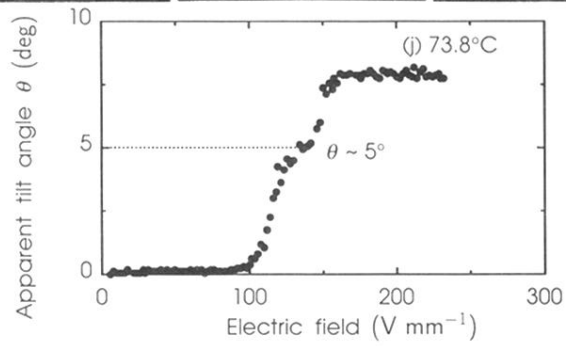
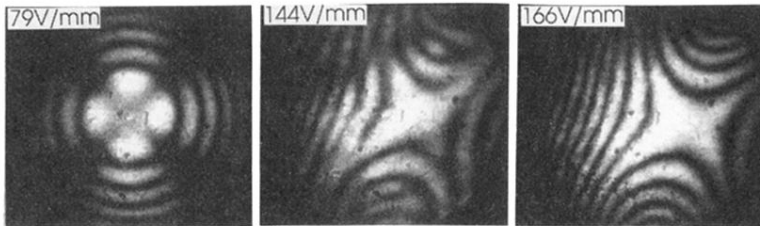
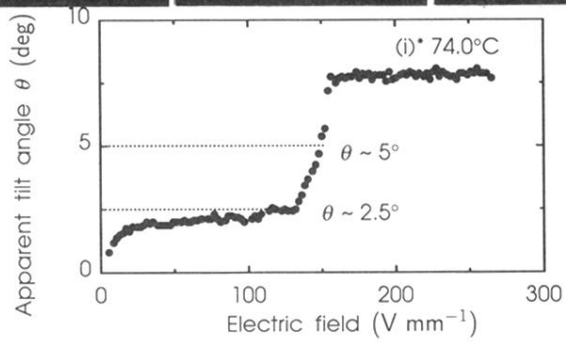
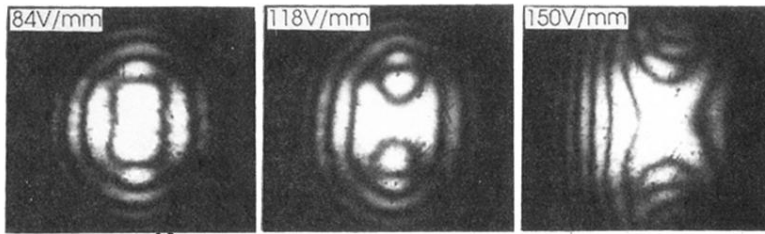


FIG. 3. (Continued).